

Recognizing Surface Properties using Impedance Perception

Ryo Kikuuwe and Tsuneo Yoshikawa

Department of Mechanical Engineering, Kyoto University
Kyoto, 606-8501 Japan

kikuuwe@ieee.org, yoshi@mech.kyoto-u.ac.jp

Abstract—When the end-effector of a robot is slid on a flat surface, the stiffness matrix obtained by linear fitting of position and force contains information not only on the stiffness coefficient and on the normal direction, but also on the friction coefficient. This paper proposes a new method for extracting information on those properties from the stiffness matrix provided by the impedance perception, which the authors previously proposed. The proposed method can be easily implemented as an encapsulated module for perception, which is separated from any control and planning methodologies. Therefore, this can be used for both autonomous and remote controlled robots, and even for monitoring a manipulation tasks performed by humans. Results of preliminary experiments are presented.

I. INTRODUCTION

In uncertain and unstructured environments, humans rely heavily on their tactile and haptic sensations. As robots broaden their field of activities toward those environments, the same kind of capability is required. Robot's haptic sensation can be composed of position (motion) and force sensing. Force sensors are no doubt a useful source of information, but in general, raw data from force sensors contain uncertainties caused by gravitation, friction effect, and so on. Several researches have been done to abstract useful information from noisy force sensor signals[1–5].

Active probing operations using an integrated perceptual and motor function(Fig.1(a)) enable efficient environment recognition[6,7]. However, this scheme contains a variety of problems to be overcome ranging from control to planning, and moreover, the primarily aimed operation must be suspended to perform the probing operation. An easier solution is to design the perceptive function as an encapsulated function, independent from the motor function, as depicted in Fig.1(b-1). This is less efficient but enables a broader range of applications; this function can be used stand-alone for monitoring the interaction between a human operator and the environment, as depicted in Fig.1(b-2). Okamura et al.'s haptic exploration [8] is a type between Fig.1(a) and (b-1). Here the robot is guided by a human and exploration is performed semi-autonomously. Dupont et al.'s research[9] is of the type of Fig.1(b-2), in which position and force data during a human's manipulation are monitored to generate environment model. The method of Fig.1(b-2) can be used for analyzing human manipulation skills[10–12].

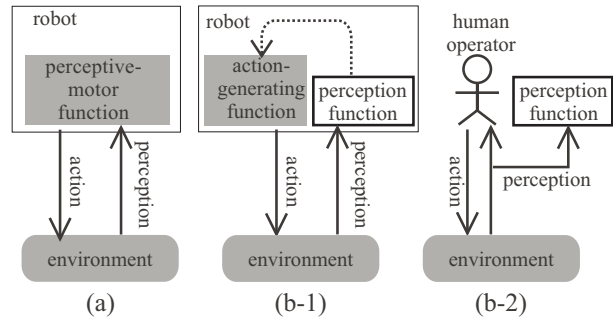


Fig. 1. Perceptive and motor functions; (a) Integrated perceptive-motor function, (b-1) Encapsulated perception function, (b-2) Perception function for monitoring actions of a human operator

In a previous paper, the authors proposed the “impedance perception” [13], which is aimed to be used in the ways of Fig.1(b-1) and (b-2). This is a technique for identifying constraint conditions based on position and force sensing during arbitrary manipulations. In this method, mechanical impedance parameters that constrain the motion of the robot's end-effector are estimated on-line in all directions at one time, and the uncertainties of the estimates are evaluated. This paper focuses on the stiffness matrix provided by this impedance perception under the situation where the end-effector is slid on a flat surface. The information of the normal direction, the stiffness and friction coefficients of the surface are extracted from the stiffness matrix. Sliding the end-effector (or the manipulated object) on an environment surface is one of the most fundamental and important operations to perceive the environment structure. The surface properties are important especially in tasks which require force control on a surface, such as polishing and drawing.

Since a stiffness matrix is estimated based on measurements during a very short time period (about 0.1[sec]), the estimates are very uncertain and unstable. Therefore some smoothing or averaging technique is necessary for fusing uncertain instantaneous data into reliable data. However, one of the disadvantages of these kinds of solutions is that they can cause time delay and insensitivity. Hence leaving this topic for future works, this research aims at exploiting instantaneous and spatially sparse observations.

In the rest of this paper, section II gives an overview of a

method to obtain the stiffness matrix using the impedance perception. Section III explains the new method for estimating surface properties, and in section IV, validity of the method is tested by experiments. Section V contains the conclusion.

II. STIFFNESS MATRIX PROVIDED BY THE IMPEDANCE PERCEPTION

In the impedance perception technique [13], the position of the robot's end-effector, $\mathbf{p}(t) \in \mathcal{R}^3$, and the force applied to the end-effector from the environment, $\mathbf{f}(t) \in \mathcal{R}^3$, are fitted to a linear dynamic equation. The recursive least squares method with forgetting factor is employed for estimating the coefficient matrices. The uncertainties of the estimates are evaluated based on the residual fitting error and distribution of the explanatory vectors, i.e., $\mathbf{p}(t)$, $\dot{\mathbf{p}}(t)$, and $\ddot{\mathbf{p}}(t)$. The Kalman filter is often used for state estimation [5], but it is not suitable for our application. One of the reasons is that, since the covariance matrix of the estimates (of state variables) is updated independently of measurements and residual errors, the matrix should not be interpreted as the uncertainty of the estimates.

The fitting equation is as follows;

$$\mathbf{f}(t) = \mathbf{c} + \mathbf{K}\mathbf{p}(t) + \mathbf{B}\dot{\mathbf{p}}(t) + \mathbf{M}\ddot{\mathbf{p}}(t), \quad (1)$$

where \mathbf{K} , \mathbf{B} and $\mathbf{M} \in \mathcal{R}^{3 \times 3}$ are the matrices of stiffness, viscosity and inertia respectively that the robot perceives. Those matrices are dependent on the dynamic properties of the end-effector and the environment, and the contact configuration between them. $\mathbf{c} \in \mathcal{R}^3$ is a constant vector which corresponds to the equilibrium point of the stiffness, a force bias resulting from the gravitation, and etc. Using Laplace transform and the bilinear transform, (1)'s discrete-time approximation is written as follows;

$$\phi_k = \Theta^T \psi_k \quad (2)$$

$$\phi_k \triangleq \mathbf{f}_k + 2\mathbf{f}_{k-1} + \mathbf{f}_{k-2} \in \mathcal{R}^3 \quad (3)$$

$$\psi_k \triangleq \begin{bmatrix} 1 & \mathbf{p}_k^T & \mathbf{p}_{k-1}^T & \mathbf{p}_{k-2}^T \end{bmatrix}^T \in \mathcal{R}^{10} \quad (4)$$

$$\Theta \triangleq \begin{bmatrix} 4\mathbf{c}^T \\ \mathbf{K}^T + 2\mathbf{B}^T/T + 4\mathbf{M}^T/T^2 \\ 2\mathbf{K}^T - 8\mathbf{M}^T/T^2 \\ \mathbf{K}^T - 2\mathbf{B}^T/T + 4\mathbf{M}^T/T^2 \end{bmatrix} \in \mathcal{R}^{10 \times 3} \quad (5)$$

where T is the sampling period and a variable with subscript k denotes its value at time instant kT .

At time instant kT , the weighted sum-of-products matrix of the residual fitting errors is written as;

$$\begin{aligned} \mathbf{J}_k(\Theta) &\triangleq \sum_{i=i_0}^k w_{k,i} (\phi_i - \Theta^T \psi_i) (\phi_i - \Theta^T \psi_i)^T \\ &= \Theta^T \mathbf{R}_k \Theta - \mathbf{Q}_k^T \Theta - \Theta^T \mathbf{Q}_k + \mathbf{F}_k \end{aligned} \quad (6)$$

where $\{w_{k,i}\}_{i_0 \leq i \leq k}$ denotes the weighting sequence at time instant kT , i_0 is the time instant at which the calculation starts, $\mathbf{R}_k \triangleq \sum_{i=i_0}^k w_{k,i} \psi_i \psi_i^T$, $\mathbf{Q}_k \triangleq$

$\sum_{i=i_0}^k w_{k,i} \psi_i \phi_i^T$, and $\mathbf{F}_k \triangleq \sum_{i=i_0}^k w_{k,i} \phi_i \phi_i^T$. The weighting is designed dependent on the speed of the movement, so that the estimate is updated more rapidly during high-speed motion of the end-effector. When \mathbf{R}_k^{-1} exists, (6) is transformed as follows;

$$\mathbf{J}_k(\Theta) = (\Theta - \hat{\Theta}_k)^T \mathbf{R}_k (\Theta - \hat{\Theta}_k) + \mathbf{S}_k \quad (7)$$

$$\hat{\Theta}_k \triangleq \mathbf{R}_k^{-1} \mathbf{Q}_k \in \mathcal{R}^{10 \times 3} \quad (8)$$

$$\mathbf{S}_k \triangleq \mathbf{F}_k - \mathbf{Q}_k^T \mathbf{R}_k^{-1} \mathbf{Q}_k \in \mathcal{R}^{3 \times 3} \quad (9)$$

Since \mathbf{R}_k is positive definite, $\mathbf{J}_k(\Theta) \succeq \mathbf{J}_k(\hat{\Theta}_k) = \mathbf{S}_k$ is satisfied for any Θ ($\mathbf{X} \succeq \mathbf{Y}$ means that $\mathbf{X} - \mathbf{Y}$ is positive semi-definite). Therefore, $\hat{\Theta}_k$ is adopted as the estimate of Θ at time instant kT .

Since $\mathbf{J}_k(\Theta) \succeq \mathbf{S}_k$, \mathbf{S}_k is the minimum of $\mathbf{J}_k(\Theta)$ in the partial order relation " \succeq ". Normalizing $\mathbf{J}_k(\Theta)$ with respect to its minimum \mathbf{S}_k , a generalized distance measure from $\hat{\Theta}_k$ to a given Θ can be defined by

$$\begin{aligned} D_{\Theta,k}(\Theta) &= \text{tr} \left(\mathbf{S}_k^{-\frac{1}{2}} (\mathbf{J}_k(\Theta) - \mathbf{S}_k) \mathbf{S}_k^{-\frac{1}{2}} \right) \\ &= \text{vec}[\Theta - \hat{\Theta}_k]^T (\mathbf{S}_k^{-1} \otimes \mathbf{R}_k) \text{vec}[\Theta - \hat{\Theta}_k], \end{aligned}$$

where \otimes denotes the Kronecker Product operator and $\text{vec}[\cdot]$ denotes the vectorization operator that stacks the columns of the argument matrix. The uncertainty bound of $\hat{\Theta}_k$ can be defined as a set of Θ 's which satisfy $D_{\Theta,k}(\Theta) < 1$, i.e.,

$$\text{vec} \left[(\Theta - \hat{\Theta}_k)^T \right] \text{vec} \left[(\Theta - \hat{\Theta}_k)^T \right]^T \preceq \mathbf{R}_k^{-1} \otimes \mathbf{S}_k. \quad (10)$$

This composes a hyper ellipsoid in \mathcal{R}^{30} space.

If $\mathbf{p}(t)$ in (1) is substituted by the true position measured by the sensors, the estimated impedance can become very unstable in rigid (or nearly rigid) contact situations. This is because the dynamic equation (1) does not hold when the position is fixed but the force varies. This problem is avoided by implementing a computer-simulated virtual visco-elastic cover around the real end-effector. The position of the *virtual soft finger* is computed by adding a simulated displacement to the real position. Using the force $\mathbf{f}(t)$ which is observed by the sensor, the virtual displacement, $\Delta \mathbf{p}_v(t)$, is simulated by solving the dynamic equation $\mathbf{f}(t) = K_v \Delta \mathbf{p}_v(t) + B_v \dot{\Delta \mathbf{p}_v}(t)$, where K_v and B_v are design parameters which represent the stiffness and viscosity coefficients of the virtual soft finger. The position of the virtual soft finger is determined by $\mathbf{p}(t) = \mathbf{p}_r(t) + \Delta \mathbf{p}_v(t)$, where $\mathbf{p}_r(t)$ denotes the real position observed by the sensors. Substituting $\mathbf{p}(t)$ in (1) with the virtual position, the estimated parameters become stable even in rigid contact states. The impedance estimated through the virtual soft finger is different from that of the real environment. It corresponds to that of the serial-coupled system of the real environment and the virtual soft finger. However, the main purpose of this method is not an accurate quantitative calibration, but

a qualitative recognition of constraint distribution over directions. Therefore, estimation through the virtual soft finger is a natural solution, in analogy with human capability of perceiving constraints even through their soft fingers or soft tools. In passive environments, the theoretical upper bound of the stiffness coefficients estimated through the virtual soft finger is K_v .

Using the above method, the estimate of the impedance matrix $\hat{\Theta}_k$ and its uncertainty bound are obtained. According to the relation (5), the estimate of the stiffness matrix \mathbf{K} is obtained by $\hat{\mathbf{K}}_k \triangleq \hat{\Theta}_k^T \mathbf{T}$ ($\in \mathcal{R}^{3 \times 3}$) where \mathbf{T} ($\in \mathcal{R}^{10 \times 3}$) is a certain constant matrix. Multiplying (10) by $\mathbf{I}_3 \otimes \mathbf{T}$ from the right and $\mathbf{I}_3 \otimes \mathbf{T}^T$ from the left yields

$$\text{vec} [\mathbf{K} - \hat{\mathbf{K}}_k] \text{vec} [\mathbf{K} - \hat{\mathbf{K}}_k]^T \preceq \mathbf{\Pi}_k, \quad (11)$$

where $\mathbf{\Pi}_k \triangleq \mathbf{P}_k \otimes \mathbf{S}_k$, $\mathbf{P}_k \triangleq \mathbf{T}^T \mathbf{R}_k^{-1} \mathbf{T}$, and \mathbf{I}_3 stands for a 3×3 identity matrix. This represents the uncertainty ellipsoid of $\hat{\mathbf{K}}_k$, and is denoted as $\hat{\mathcal{E}}_k$. A generalized distance measure from $\hat{\mathbf{K}}_k$ to a given \mathbf{K} can be defined by

$$D_k(\mathbf{K}) \triangleq \text{vec} [\mathbf{K} - \hat{\mathbf{K}}_k]^T \mathbf{\Pi}_k^{-1} \text{vec} [\mathbf{K} - \hat{\mathbf{K}}_k]. \quad (12)$$

III. ESTIMATING SURFACE PROPERTIES

When the end-effector is in contact with a single flat surface, the stiffness matrix provided by the impedance perception contains information not only on the stiffness coefficient and on the normal direction, but also on the friction coefficient. This section discusses a method to extract information of those properties.

Generally the stiffness matrix $\hat{\mathbf{K}}$ provided by the impedance perception is not feasible for a dynamic friction state. Therefore, a calculation is performed to find a new estimate of the stiffness matrix which is consistent with a dynamic friction state and is sufficiently close to $\hat{\mathbf{K}}$. Moreover, an ellipsoidal uncertainty bound accompanying with the new estimate is defined. Based on this stiffness matrix and its uncertainty ellipsoid, the surface properties and their uncertainties are obtained.

A. Stiffness Matrix and Surface Properties

Let \mathbf{n} denote the normal direction and \mathbf{t} denote one of the tangential directions in which the friction force acts. \mathbf{n} and \mathbf{t} are orthogonal to each other. Let \mathbf{p} ($\in \mathcal{R}^3$) be the position of the end-effector, and \mathbf{f} ($\in \mathcal{R}^3$) be the force applied from the end-effector to the environment. Then, the stiffness in the surface normal direction causes the relation $\mathbf{n}^T \delta \mathbf{f} = \kappa (\mathbf{n}^T \delta \mathbf{p})$, and the Coulomb friction causes the relation $\mathbf{t}^T \delta \mathbf{f} = \mu (\mathbf{n}^T \delta \mathbf{f})$. Here, δ denotes a small change in the associated variable and κ and μ are stiffness and friction coefficients, respectively, of the surface. \mathbf{p} is substituted by the virtual position $\mathbf{p}(t)$, not

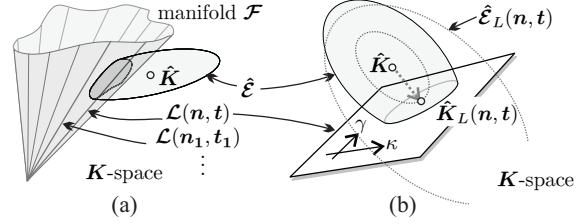


Fig. 2. Inclusive relationship among subsets of $\{\mathbf{K} \in \mathcal{R}^{3 \times 3}\}$

by the real position $\mathbf{p}_r(t)$. These relations between $\delta \mathbf{p}$ and $\delta \mathbf{f}$ are rewritten as follows;

$$\begin{bmatrix} \mathbf{n}^T \\ \mathbf{t}^T \end{bmatrix} \delta \mathbf{f} = \begin{bmatrix} \kappa \\ \kappa \mu \end{bmatrix} \mathbf{n}^T \delta \mathbf{p} \quad (13)$$

Thus, the stiffness matrix, which relates $\delta \mathbf{f}$ and $\delta \mathbf{p}$ in the form of $\delta \mathbf{f} = \mathbf{K} \delta \mathbf{p}$, can be described by

$$\mathbf{K} = \begin{bmatrix} \mathbf{n} & \mathbf{t} \end{bmatrix} \boldsymbol{\lambda} \mathbf{n}^T, \quad (14)$$

where $\boldsymbol{\lambda} = [\kappa, \gamma]^T$, $\gamma \triangleq \kappa \mu$.

The discussion above shows that the force-position relation in a dynamic friction situation on a flat surface is determined by the stiffness matrix (14). Letting $\mathcal{L}(\mathbf{n}, \mathbf{t})$ be a set of \mathbf{K} 's which can be expressed by (14) using a given pair $\{\mathbf{n}, \mathbf{t}\}$, $\mathcal{L}(\mathbf{n}, \mathbf{t})$ constitutes a 2 dimensional subspace of $\{\mathbf{K} \in \mathcal{R}^{3 \times 3}\}$, in which the coordinates can be parameterized by two variables $\{\kappa, \gamma\}$. Moreover, letting \mathcal{F} be a set of all \mathbf{K} 's which can be written by (14), \mathcal{F} is the union of all $\mathcal{L}(\mathbf{n}, \mathbf{t})$'s, and is a 5 dimensional manifold, as shown in Fig.2(a).

B. New Estimate $\hat{\mathcal{E}}_L(\mathbf{n}, \mathbf{t})$ with a Fixed $\{\mathbf{n}, \mathbf{t}\}$.

Generally $\hat{\mathbf{K}}$, which is provided by the impedance perception, is not an element of \mathcal{F} . Therefore, it is necessary to find an element of \mathcal{F} which is close from $\hat{\mathbf{K}}$, and to define a new uncertainty ellipsoid centered at it. In the discussion below, the subscripts that denote time index (e.g. k and i) are dropped for brevity.

Letting $\mathbf{L} = \mathbf{n} \otimes [\mathbf{n}, \mathbf{t}] \in \mathcal{R}^{9 \times 2}$, $\mathbf{K} \in \mathcal{L}$ can be written as $\text{vec}[\mathbf{K}] = \mathbf{L} \boldsymbol{\lambda}$. Under the condition $\mathbf{K} \in \mathcal{L}$, (12) can be rewritten as

$$D(\mathbf{K}) = (\boldsymbol{\lambda} - \hat{\boldsymbol{\lambda}}_L)^T \mathbf{V}_L^{-1} (\boldsymbol{\lambda} - \hat{\boldsymbol{\lambda}}_L) + \hat{D}_L \quad (15)$$

$$\hat{\boldsymbol{\lambda}}_L \triangleq \mathbf{V}_L \mathbf{h} \quad (16)$$

$$\hat{D}_L \triangleq \hat{\mathbf{k}}^T \mathbf{\Pi}^{-1} \hat{\mathbf{k}} - \mathbf{h}^T \mathbf{V}_L \mathbf{h}, \quad (17)$$

where $\hat{\mathbf{k}} = \text{vec}[\hat{\mathbf{K}}]$, $\mathbf{V}_L \triangleq (\mathbf{L}^T \mathbf{\Pi}^{-1} \mathbf{L})^{-1}$, and $\mathbf{h} \triangleq \mathbf{L}^T \mathbf{\Pi}^{-1} \hat{\mathbf{k}}$. Letting $\hat{\mathbf{K}}_L$ be the element of \mathcal{L} which has the minimum generalized distance from $\hat{\mathbf{K}}$ (Fig.2(b)), this is written as $\hat{\mathbf{K}}_L = \begin{bmatrix} \mathbf{n} & \mathbf{t} \end{bmatrix} \hat{\boldsymbol{\lambda}}_L \mathbf{n}^T$. \hat{D}_L is the generalized distance from $\hat{\mathbf{K}}_L$ to $\hat{\mathbf{K}}$. Note that $\hat{\boldsymbol{\lambda}}_L$, \hat{D}_L , \mathbf{V}_L , and $\hat{\mathbf{K}}_L$ are functions of $\{\mathbf{n}, \mathbf{t}\}$.

The uncertainty ellipsoid accompanied by $\hat{\mathbf{K}}_L(\mathbf{n}, \mathbf{t})$ can be defined by moving $\hat{\mathcal{E}}$ from $\hat{\mathbf{K}}$ to $\hat{\mathbf{K}}_L$, and

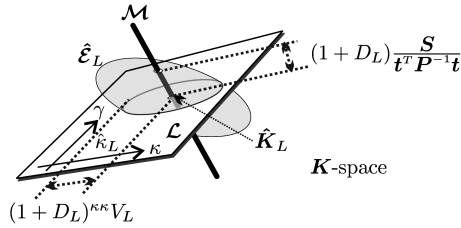


Fig. 3. Evaluation of feasibility of $\hat{\mathcal{E}}_L(\mathbf{n}, \mathbf{t})$

magnifying it with respect to \hat{D}_L . This new ellipsoidal bound, to be denoted by $\hat{\mathcal{E}}_L(\mathbf{n}, \mathbf{t})$, is represented by an inequality

$$\text{vec}[\mathbf{K} - \hat{\mathbf{K}}_L] \text{vec}[\mathbf{K} - \hat{\mathbf{K}}_L]^T \preceq (1 + \hat{D}_L) \mathbf{\Pi}. \quad (18)$$

C. Feasibility of $\hat{\mathcal{E}}_L(\mathbf{n}, \mathbf{t})$

In the previous subsection, $\hat{\mathbf{K}}_L(\mathbf{n}, \mathbf{t})$, the element of $\mathcal{L}(\mathbf{n}, \mathbf{t})$ closest from $\hat{\mathbf{K}}$, and its accompanying uncertainty ellipsoid $\hat{\mathcal{E}}_L(\mathbf{n}, \mathbf{t})$ are given. The feasibility of the pair $\{\mathbf{n}, \mathbf{t}\}$ can be evaluated by the shape, size, and location of $\hat{\mathcal{E}}_L(\mathbf{n}, \mathbf{t})$. \mathbf{n} is reliably a normal direction when $\kappa \gg 0$. \mathbf{t} is reliably a tangential direction when $\mathbf{K}\mathbf{t} \approx \mathbf{0}_3$. This subsection introduces a maximization criterion $\Phi(\mathbf{n}, \mathbf{t})$ which evaluates the feasibility of $\hat{\mathcal{E}}_L(\mathbf{n}, \mathbf{t})$.

Firstly, a feasibility criterion for \mathbf{n} direction is introduced. Considering (15), the cross-section of the hyper ellipsoid $\hat{\mathcal{E}}_L(\mathbf{n}, \mathbf{t})$ with the hyper plane $\mathcal{L}(\mathbf{n}, \mathbf{t})$ is an ellipsoid represented by

$$(\lambda - \hat{\lambda}_L)^T \mathbf{V}_L^{-1} (\lambda - \hat{\lambda}_L) \leq 1 + \hat{D}_L. \quad (19)$$

The value range of κ under the condition of (19) is

$$(\kappa - \hat{\kappa}_L)^2 \leq (1 + \hat{D}_L)^{\kappa} V_L, \quad (20)$$

where $\hat{\kappa}_L$ is the 1st element of $\hat{\lambda}_L$ and ${}^{\kappa} V_L$ is the (1, 1)-th element of \mathbf{V}_L (Fig.3). Therefore, when the following function is large, $\kappa \gg 0$ is reliably satisfied;

$$\Phi_{\mathbf{n}}(\mathbf{n}, \mathbf{t}) = \frac{\max(0, \hat{\kappa}_L(\mathbf{n}, \mathbf{t}))^2}{(1 + \hat{D}_L(\mathbf{n}, \mathbf{t}))^{\kappa} V_L(\mathbf{n}, \mathbf{t})} \quad (21)$$

Secondly, a feasibility criterion for \mathbf{t} direction is introduced. The reliability of $\mathbf{K}\mathbf{t} = (\mathbf{t}^T \otimes \mathbf{I}_3) \text{vec}[\mathbf{K}] \approx \mathbf{0}_3$ can be evaluated by the size of the cross section ellipsoid of $\hat{\mathcal{E}}_L$ with the hyper plane

$$\mathcal{M} \triangleq \left\{ \mathbf{K} \mid \text{vec}[\mathbf{K}] = \text{vec}[\hat{\mathbf{K}}_L] + (\mathbf{t} \otimes \mathbf{I}_3) \boldsymbol{\xi}, \boldsymbol{\xi} \in \mathcal{R}^3 \right\},$$

which includes $\hat{\mathbf{K}}_L$ (Fig.3). The value range of $\boldsymbol{\xi}$ in the cross-section ellipsoid $\mathcal{M} \cap \hat{\mathcal{E}}_L$ is given by

$$\boldsymbol{\xi} \boldsymbol{\xi}^T \preceq (1 + \hat{D}_L) \mathbf{S} / (\mathbf{t}^T \mathbf{P}^{-1} \mathbf{t}). \quad (22)$$

The size of this ellipsoid can be evaluated by the trace of the matrix in the right-hand term, and when this is small,

$\mathbf{K}\mathbf{t} \approx \mathbf{0}_3$ can be said to reliably holds. Therefore, the criterion below can be given;

$$\Phi_{\mathbf{t}}(\mathbf{n}, \mathbf{t}) = \frac{\mathbf{t}^T \mathbf{P}^{-1} \mathbf{t}}{(1 + \hat{D}_L(\mathbf{n}, \mathbf{t})) \text{tr} \mathbf{S}}. \quad (23)$$

According to the discussion above, the feasibility criterion for $\hat{\mathcal{E}}_L(\mathbf{n}, \mathbf{t})$ can be given by $\Phi(\mathbf{n}, \mathbf{t}) = \Phi_{\mathbf{n}}(\mathbf{n}, \mathbf{t}) \Phi_{\mathbf{t}}(\mathbf{n}, \mathbf{t})$. Let $\{\hat{\mathbf{n}}, \hat{\mathbf{t}}\}$ denote the pair $\{\mathbf{n}, \mathbf{t}\}$ which maximizes $\Phi(\mathbf{n}, \mathbf{t})$.

D. Convergence Calculation to Obtain $\hat{\mathcal{E}}_F$

By searching for the pair $\{\mathbf{n}, \mathbf{t}\}$ which maximizes the criterion $\Phi(\mathbf{n}, \mathbf{t})$, the most feasible estimate $\hat{\mathcal{E}}_F$ can be obtained. However, it is not easy to rigorously solve this maximization problem. To reduce the computation time, an approximate convergence calculation is performed.

Usually, the stiffness coefficient is most reliably estimated in the direction in which the position variance is largest, that is, the direction in which the end-effector moves. Therefore, the direction $\boldsymbol{\tau}$ with which $\mathbf{K}\boldsymbol{\tau} \approx \mathbf{0}_3$ holds most reliably is a good candidate for the projection of the moving direction onto the surface, i.e. for the direction \mathbf{t} . Multiplying (11) by $\boldsymbol{\tau}^T \otimes \mathbf{I}_3$ from the left and $\boldsymbol{\tau} \otimes \mathbf{I}_3$ from the right yields $(\mathbf{K}\boldsymbol{\tau} - \hat{\mathbf{K}}\boldsymbol{\tau})(\mathbf{K}\boldsymbol{\tau} - \hat{\mathbf{K}}\boldsymbol{\tau})^T \preceq \boldsymbol{\tau}^T \mathbf{P} \boldsymbol{\tau} \otimes \mathbf{S}$. Substituting this by $\mathbf{K}\boldsymbol{\tau} = \mathbf{0}_3$ yields $\hat{\mathbf{K}}\boldsymbol{\tau}(\hat{\mathbf{K}}\boldsymbol{\tau})^T \preceq \boldsymbol{\tau}^T \mathbf{P} \boldsymbol{\tau} \otimes \mathbf{S}$. Let $\hat{\boldsymbol{\tau}}$ denote the vector $\boldsymbol{\tau}$ which minimizes $(\boldsymbol{\tau}^T \hat{\mathbf{K}}^T \mathbf{S}^{-1} \hat{\mathbf{K}} \boldsymbol{\tau}) / (\boldsymbol{\tau}^T \mathbf{P} \boldsymbol{\tau})$. Then, $\hat{\boldsymbol{\tau}}$ can be analytically found, and can be used as an initial temporary estimate for \mathbf{t} . Starting from $\hat{\boldsymbol{\tau}}$, the following numerical calculations are performed;

- 1) Search for \mathbf{n} which maximizes $\Phi(\mathbf{n}, \hat{\boldsymbol{\tau}})$ subject to $\mathbf{n} \perp \hat{\boldsymbol{\tau}}$, and let it be denoted by \mathbf{n}' .
- 2) Letting $\mathbf{v}' := \mathbf{n}' \times \hat{\boldsymbol{\tau}}$, search for $\{\mathbf{n}, \mathbf{t}\}$ which maximizes $\Phi(\mathbf{n}, \mathbf{t})$ subject to $\mathbf{n}, \mathbf{t} \perp \mathbf{v}'$, and let it be denoted by $\{\mathbf{n}'', \mathbf{t}''\}$.
- 3) Starting from $\{\mathbf{n}'', \mathbf{t}''\}$, search for an extremum of $\Phi(\mathbf{n}, \mathbf{t})$ by the steepest gradient method.

By the procedure above, the final solution $\{\hat{\mathbf{n}}, \hat{\mathbf{t}}\}$ is obtained. The final estimates of κ and μ are given as $\hat{\kappa} \triangleq \hat{\kappa}_L(\hat{\mathbf{n}}, \hat{\mathbf{t}})$ and $\hat{\mu} \triangleq \hat{\gamma}_L(\hat{\mathbf{n}}, \hat{\mathbf{t}}) / \hat{\kappa}_L(\hat{\mathbf{n}}, \hat{\mathbf{t}})$ respectively, where $\hat{\gamma}_L(\hat{\mathbf{n}}, \hat{\mathbf{t}})$ is the 2nd element of $\hat{\lambda}_L(\hat{\mathbf{n}}, \hat{\mathbf{t}})$. The uncertainty region of $\hat{\kappa}$ is given by substituting (20) by $\{\hat{\mathbf{n}}, \hat{\mathbf{t}}\}$. That of $\hat{\mu}$, on the other hand, is given by $(\mu - \hat{\mu})^2 \leq (1 + \hat{D}_L(\hat{\mathbf{n}}, \hat{\mathbf{t}})) ({}^{\gamma\gamma} V_L(\hat{\mathbf{n}}, \hat{\mathbf{t}})) / \hat{\kappa}^2$, where ${}^{\gamma\gamma} V_L$ is the (2, 2)-th element of \mathbf{V}_L .

IV. EXPERIMENT

A. Setup and Method

Preliminary experiments were conducted. The overview of the setup is show in Fig.4. It consists of a three-joint miniature robot arm ‘‘Mini-Robot’’ (Daikin Industries Ltd.), a 6-axis force-torque sensor (‘‘NANO Sensor’’, BL Autotec, LTD.), and an acrylic ball (diameter 38[mm], a

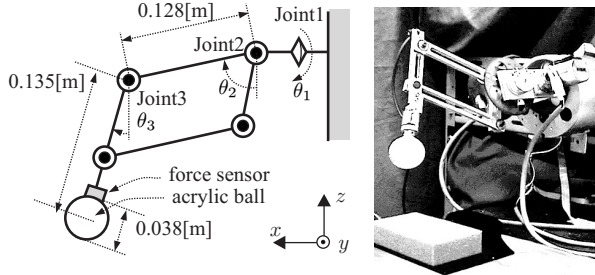


Fig. 4. Dimensions of the setup

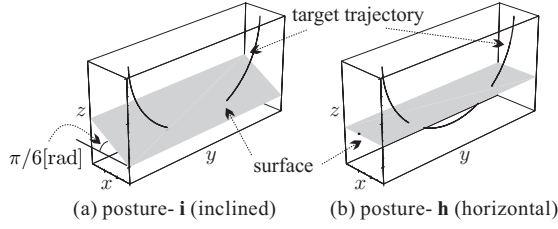


Fig. 5. Surface postures and the target trajectories

table tennis ball), which is used as an end-effector. The robot arm is a parallel link mechanism connected to the base through a rotational joint. The position of the end-effector is measured by the optical encoders (500P/R type) which are attached to the joint actuators through reduction gears (ratio 1:8).

As shown in Fig.5, in the experiments, the end-effector is moved along a semicircular target trajectory, using ordinary PD control (200[N/m] for P gain, 2.0[Ns/m] for D gain) in Cartesian space. Three types of surfaces are used; a sponge (S), an acrylic board (A), and a metal file (F). The surfaces are located in two different postures; 30-degree-inclined (posture-i) and horizontal (posture-h). When the target position is below the surface, the end-effector is slid on the surface and a compliant force is applied on it. The experiments were conducted in six cases; **iA**, **iF**, **iS**, **hA**, **hF**, and **hS**.

The control and measurement are performed by a computer with an Intel Pentium III CPU (1[GHz]). The sampling period of the impedance perception is 2[msec], and that of the surface property estimation is 10[msec]. The sensor data of the position and force are filtered by 4th order Butterworth low-pass filters with cutoff frequency 50[Hz]. The stiffness and viscosity of the virtual soft finger, K_v and B_v , are set to be 700[N/m] and 10[Ns/m] respectively. The weightings of the measurements ($w_{k,i}$ in (6)) are reduced to a half after the 1.0×10^{-3} [m] of distance or 0.1[sec] of time is moved or elapsed.

The friction coefficients of the surfaces **A**, **F**, and **S** are approximately 0.15, 0.45, and 0.41 respectively. The surfaces **A** and **F** are almost rigid, thus the apparent stiffness coefficients estimated through the virtual soft finger are

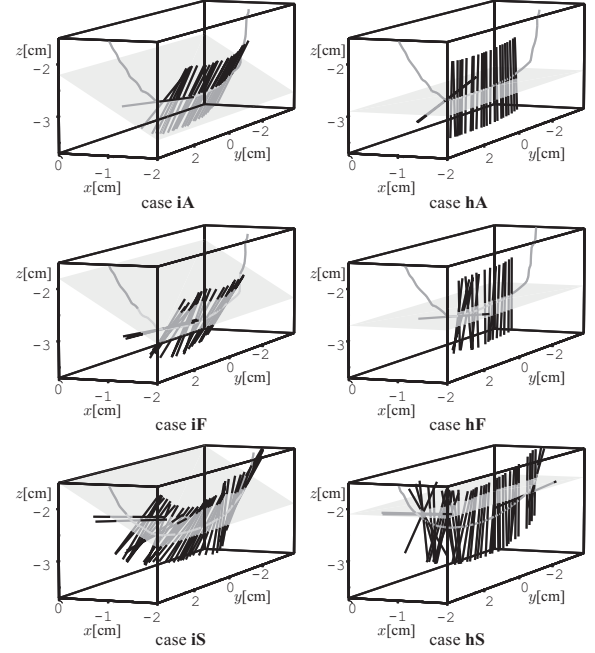


Fig. 6. Estimated normal directions \hat{n}

expected to be equal to $K_v = 700$ [N/m]. The stiffness coefficient of the surface **S** is approximately 260[N/m], thus its apparent stiffness coefficient is expected to be $260K_v/(260 + K_v) \approx 189$ [N/m].

B. Result

The experimental results are shown in Fig.6 and Fig.7. Fig.6 shows the estimated normal direction, \hat{n} , and the trajectory of the end-effector, $p_r(t)$. The transparent planes in Fig.6 represent the position of the object surfaces by actual measurement. On the other hand, Fig.7 shows the estimated stiffness and friction coefficients, \hat{k} and $\hat{\mu}$. Estimated values are represented by black solid curves and their uncertainties are represented by gray bands. The time spans in which the end-effector is in touch with the surfaces are bounded by the vertical lines (those represent the discontinuities detected by the impedance perception[13]). Those discontinuities agree with the actual times of contact and separation with the surface. When the discontinuities are detected, the cumulated data of the past, R_k , Q_k and F_k are reset to zero). The proposed algorithm of the surface properties estimation (in the section III) is performed only when $\hat{E} \neq O_{3 \times 3}$, i.e. $\hat{k}^T \Pi^{-1} \hat{k} > 1$. Thus it is performed only when the end-effector is in touch with the surface. The position of the surface is adjusted so that the maximum force applied on the object is around 1.8[N]. Thus the fixed position of the surface and the length of the period in which the end-effector is in touch with the surface are dependent on the stiffness of the surface.

Fig.6 shows that the normal directions are properly esti-

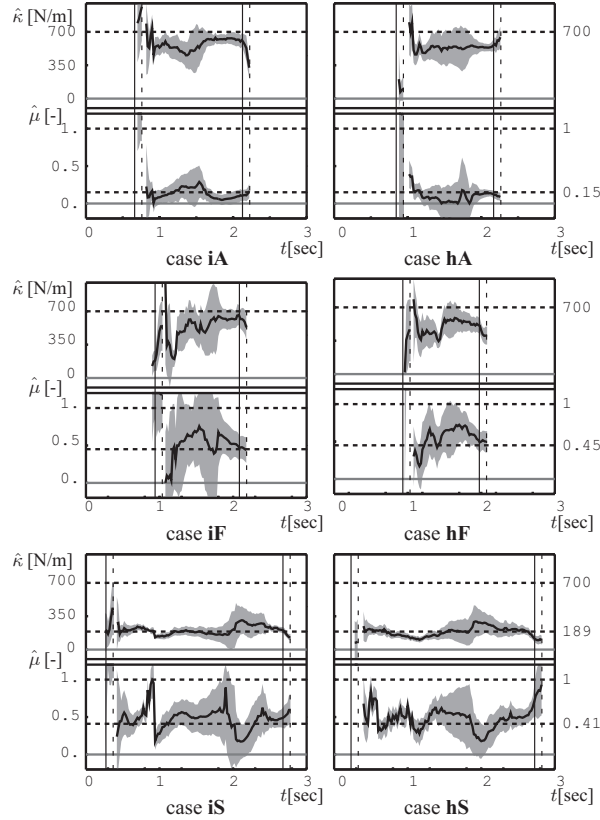


Fig. 7. Estimated stiffness and friction coefficients

mated, though the surface **S**, which significantly deforms, slightly disturbs the estimates. Some misestimations follow the collisions, but these are limited in the short time periods since when a discontinuity occurs until when that is detected.

Fig.7 shows that, since the surfaces **A** and **F** are almost rigid, thus the stiffness coefficients, $\hat{\kappa}$, of **iA**, **hA**, **iF**, **hF** are estimated to be large, around the virtual soft finger's limit $K_v = 700[\text{N/m}]$. On the other hand, since the surface **S** is soft, thus $\hat{\kappa}$ in **iS** and **hS** has small values and it is close to $189[\text{N/m}]$ as expected. The friction coefficient, $\hat{\mu}$, of all the surfaces are properly estimated. Those of the surfaces **A** and **F** are distinctly different. Same surfaces with different postures result in almost same values of $\hat{\kappa}$ and $\hat{\mu}$. This indicates the validity of the proposed method.

V. CONCLUSION

This paper proposed a method for identifying environment surface properties, including the normal direction, and the stiffness and friction coefficients, based on the stiffness matrix provided by the impedance perception. The validity of the method was tested by experiments. As a future topic, it is necessary to seek some methods for integrating uncertain data in the time direction to obtain reliable information. Further research will be directed

toward constructing the model of the environment, which can be used for simulation and/or virtual reality.

Though the main purpose of this method is to obtain qualitative information including uncertainty, the precision and accuracy of the estimation must be evaluated quantitatively. The influences of the design parameters on the accuracy of the estimation must be clarified, especially for an optimal design of the forgetting factors and the virtual soft finger. This is a future topic.

VI. REFERENCES

- [1] B. Eberman and J. K. Salisbury, "Application of Change Detection to Dynamic Contact Sensing," *Int. J. of Robotics Research*, vol. 13, no. 5, pp. 369–394, 1994.
- [2] M. Skubic and R. A. Volz, "Identifying Single-Ended Contact Formations from Force Sensor Patterns," *IEEE Trans. of Robotics and Automation*, vol. 16, no. 5, pp. 597–602, 2000.
- [3] B. J. McCarragher and H. H. Asada, "Qualitative Template Matching Using Dynamic Process Models for State Transition Recognition of Robotic Assembly," *J. of Dynamic Systems, Measurement, and Control*, vol. 115, pp. 261–269, 1993.
- [4] G. E. Hovland and B. J. McCarragher, "Hidden Markov Models as a Process Monitor in Robotic Assembly," *Int. J. of Robotics Research*, vol. 17, no. 2, pp. 153–168, 1998.
- [5] J. De Schutter, H. Bruyninckx, S. Dutre, and J. D. Geeter, "Estimating First-Order Geometric Parameters and Monitoring Contact Transitions during Force-Controlled Compliant Motion," *Int. J. of Robotics Research*, vol. 18, no. 12, pp. 1161–1184, 1999.
- [6] T. Yoshikawa, Y. Yu, and M. Koike, "Estimation of Contact Position between Object and Environment Based on Probing of Robot Manipulator," in *Proc. of the 1996 IEEE/RSS Int. Conf. on Intelligent Robots and Systems*, 1996, vol. 2, pp. 769–776.
- [7] T. Mouri, T. Yamada, N. Mimura, and Y. Funahashi, "Identification of Contact Conditions from Contaminated Data of Contact Moment," in *Proc. of the 1999 IEEE Int. Conf. of Robotics and Automation*, 1999, pp. 585–591.
- [8] A. M. Okamura, M. A. Costa, M. L. Turner, and C. Richard, "Haptic Surface Exploration," in *Experimental Robotics VI*, P. Corke and J. Trevelyan, Eds., vol. 250 of *Lect. Notes in Control and Information Sciences*, pp. 423–432. Springer-Verlag, 2000.
- [9] P. Dupont, T. M. Schuteis, P. A. Millman, and R. D. Howe, "Automatic Identification of Environment Haptic Properties," *Presence*, vol. 8, no. 4, pp. 394–411, 1999.
- [10] G. E. Hovland, P. Sikka, and B. J. McCarragher, "Skill Acquisition from Human Demonstration Using a Hidden Markov Model," in *Proc. of the 1996 IEEE Int. Conf. of Robotics and Automation*, 1996, pp. 2706–2711.
- [11] B. J. McCarragher, "Force Sensing from Human Demonstration Using a Hybrid Dynamical Model and Qualitative Reasoning," in *Proc. of the 1994 IEEE Int. Conf. of Robotics and Automation*, 1994, pp. 557–563.
- [12] M. Skubic and R. A. Volz, "Acquiring Robust, Force-Based Assembly Skills from Human Demonstration," *IEEE Trans. of Robotics and Automation*, vol. 16, no. 6, pp. 772–781, 2000.
- [13] R. Kikuuwe and T. Yoshikawa, "Robot Perception of Environment Impedance," in *Proc. of the 2002 IEEE Int. Conf. of Robotics and Automation*, 2002, pp. 1661–1666.